A&A 435, 449–457 (2005)
DOI: 10.1051/0004-6361:20041623

Astronomy & Astrophysics

The *XMM-Newton* view of PG quasars

II. Properties of the Fe K_α line

E. Jiménez-Bailón, E. Piconcelli, M. Guainazzi, N. Schartel, P. M. Rodríguez-Pascual, and M. Santos-Lleó

XMM-Newton Science Operation Center/RSSD–ESA, Apartado 50727, 28080 Madrid, Spain
e-mail: ejimenez@xmm.vilspa.esa.es

Received 8 July 2004 / Accepted 21 December 2004

Abstract. The properties of the fluorescence Fe K_α emission lines of a sample of 38 quasars (QSOs) observed with *XMM-Newton* are studied. These objects are included in the optically selected sample from the Palomar-Green (PG) Bright Quasar Survey with an X-ray luminosity $1.3 \times 10^{43} < L_{2-10\,\mathrm{keV}} < 5.1 \times 10^{45}$ erg s^{-1} and $z \leq 1.72$. For each object in the sample, we investigated the presence of both narrow and broad iron lines in detail. A total of 20 out of the 38 QSOs show evidence of an Fe K_α emission line with a narrow profile. The majority of the lines are consistent with an origin in low ionization material, which is likely to be located in the outer parts of the accretion disk, the molecular torus, and/or the Broad Line Region. The average properties of the narrow Fe K_α emission line observed in the sample are similar to those of Seyfert type galaxies as inferred from recent *XMM-Newton* and *Chandra* studies. A broad line has been significantly detected in only three objects. Furthermore, we studied the relationship between the equivalent width (*EW*) of the iron line and the hard band X-ray luminosity for radio quiet quasars. The analysis indicates that no clear correlation between the strength of the line and the hard X-ray luminosity is present, and our results do not show compelling evidence for an anticorrelation between these two quantities, i.e. the so-called *X-ray Baldwin effect*.

Key words. galaxies: active – galaxies: nuclei – quasar: general – X-rays: galaxies

1. Introduction

The iron K_α emission line was one of the first atomic features discovered in X-ray spectra of active galaxies (Mushotzky et al. 1978). Its origin was promptly interpreted as photoelectric absorption followed by fluorescence emission (see Reynolds & Nowak 2003, for a review). The combination of fluorescent yield ($\propto Z^4$) and the (relatively) high abundance of iron justifies the strength of such a feature with respect to lines emitted by other atomic species. The K_α line actually consists of two different lines that correspond to the 2p→1s transition and that, in the case of "neutral" iron (i.e. FeI–XVII), have an energy of 6.404 and 6.391 keV, respectively.

However, the resolving power of earlier X-ray spectrometers does not allow for separating both features (but see also Kaspi et al. 2002, for results with *Chandra* HETGS), so they are usually observed (and considered) as a single emission feature. The maximum energy for this line is 6.97 keV corresponding to emission from H-like iron.

The X-ray spectral survey of Seyfert galaxies carried out with *Ginga* (Nandra & Pounds 1994) found this feature in the vast majority of these sources. In the same years, several theoretical works suggested an origin for this feature in circumnuclear optically-thick material (i.e. the disk and/or the molecular torus), together with X-ray Compton reflection (George & Fabian 1991; Matt et al. 1991; Krolik et al. 1994; Ghisellini et al. 1994)

The study of the iron K_α emission line became one of priorities of X-ray astronomy after the discovery of a line with a broadened and skewed profile in the *ASCA* spectrum of MCG–6-30-15 and (Tanaka et al. 1995). Such a broad profile was interpreted as the combination of transverse Doppler shift, relativistic beaming, and gravitational redshift. It was the first direct evidence of emission from an accretion disk extending down to very few Schwarzschild radii from a supermassive blackhole. Iron lines are therefore a unique tool for studying strong gravity effects and mapping the innermost regions of the accretion flow.

The advent of *XMM-Newton* and *Chandra* has allowed more detailed investigations of this spectral feature and provided important insights into its properties. In particular, Yaqoob & Padmanabhan (2004) and Pounds & Reeves (2002) pointed out the ubiquity of an unresolved Fe K_α line in the spectra of bright Seyfert galaxies. Such a line should therefore emerge from the outermost regions of the accretion disk, but non-disk contributions (i.e. from the Broad Line Region Yaqoob et al. 2001) are also plausible. Contrary to previous low-resolution *ASCA* observations (Nandra et al. 1997) iron emission lines with a broad profile appear to be quite rare in *Chandra* and *XMM-Newton* observations.

It is worth noting that the Fe K_α line has not commonly been observed in the X-ray spectra of high luminosity AGNs (i.e. QSOs) and, when detected, it is usually weaker than in Seyfert galaxies (Reeves & Turner 2000). To explain this effect, Iwasawa & Taniguchi (1993) suggested, based on *Ginga* data, the existence of an X-ray "Baldwin effect" such that, as the X-ray luminosity increases, the upper layers of the disk become progressively more ionized until any reprocessed feature is suppressed (Ross et al. 1999). The X-ray Baldwin effect was also observed with *ASCA* (Nandra et al. 1997) and more recently with *XMM-Newton* (Page et al. 2004a). However, due to selection effects (i.e. relative faintness, lower density surface than in Seyfert galaxies) and to the limited spectral capabilities of past X-ray telescopes, knowledge about the properties of the iron emission line in QSOs is quite sparse.

Our extensive *XMM-Newton* program (Piconcelli et al. 2005) is designed to fill this lack of information by detailed and uniform analysis of 40 *EPIC* spectra of optically-bright QSOs selected from the Palomar-Green survey (Schmidt & Green 1983). With such a large sample we aim to provide useful insights into the characteristics of the Fe K_α line and its origin. Furthermore, the homogeneity of our sample strongly prevents possible biases due to mixing different classes of AGNs (see Sect. 4).

2. *XMM-Newton* observation

This study presents an analysis of the iron *K* band of all public observations of PG quasars available in the *XMM-Newton* Science Archive (XSA) as of February 2004. Out of the 42 original objects, two (0003+199 and 1426+015) were excluded due to large pile–up and two others (1001+054 and 1404+226) due to low statistics in the hard X-ray band, i.e. >2 keV. The spectra were obtained by processing the *XMM-Newton* observations using the Science Analysis System (SAS) v.5.4.1. Sample properties and data reduction are described in detail in Piconcelli et al. (2005). *MOS1* and *MOS2* 0.6–10 keV spectra were combined and analyzed simultaneously with 0.3–12 keV *pn* spectrum.

3. Analysis of spectra

3.1. Best fit models

The spectrum of each QSO was analyzed using XSPEC v.11.2, (Arnaud 1996). From Piconcelli et al. (2004), we obtained the best fit model for the continuum emission of each QSO studied.

Table 1 shows the best fit model obtained for each source. A complete description of these models and their parameters are presented in Piconcelli et al. (2005). In the following, all the energies of the QSOs are referred to the rest frame, and errors are given to the 90 per cent confidence level (i.e. $\Delta\chi^2 = 2.71$) unless otherwise stated. Luminosities were calculated considering a flat cosmology with $(\Omega_M, \Omega_\Lambda) = (0.3, 0.7)$ and $H_0 = 70\ \mathrm{km\,s^{-1}\ Mpc^{-1}}$ (Bennett et al. 2003).

3.2. Spectral models for the Fe line

First, we investigate the presence of fluorescent Fe emission lines by adding an unresolved narrow Gaussian line[1] to the best fit models reported in Piconcelli et al. (2005). Whenever the addition of this component was not required by the data (i.e. its significance is <95% according to an *F*-test), we then fixed the centroid of the line to 6.4 keV. In such way an estimate of upper limit to the rest-frame equivalent width (*EW*) of the neutral iron fluorescence emission was inferred. The best-fit values for the emission line parameters are listed in Table 1. An iron fluorescent emission line with a narrow profile is significantly detected, i.e. with an *F*-test criterion at a significance level of ≥95%, in 20 QSOs (17 radio quiet and 3 radio loud).

Figure 1a shows the centroid of the iron fluorescence narrow emission line plotted as a function of 2–10 keV luminosity for the 20 QSOs with significant detection of such an emission feature (see Table 1). There is no apparent trend with luminosity or radio-loudness. The centroid energy of the Fe K_α line in all but four quasars (1115+407 1116+215 1244+026 1402+261) corresponds to low ionization states, i.e. Fe I–XVII (Makishima 1986). Figure 1b shows the *EW* of Fe K-shell narrow emission lines as a function of luminosity in the hard band; however; however no obvious correlation emerges from this plot (see Sect. 4.2.1).

Besides the ubiquitous presence of a narrow Fe emission line centered at ~6.4 keV, recent works based on Seyfert 1 samples observed with both the *Chandra* (Yaqoob & Padmanabhan 2004) and *XMM-Newton* (Pounds & Reeves 2002) high signal-to-noise spectroscopic data have found in some objects evidence of additional underlying broad and skewed emission supporting the original *ASCA* claims for a relativistically broadened component (Nandra et al. 1997). Consequently, we added a disk line to the fitting model to account for any such "broad" component. For this we used the `LAOR` model following recent *XMM-Newton* results that advocate a spinning black hole in nearby Seyfert galaxies (Wilms et al. 2001; Fabian 2002). In our fit we assumed a fixed rest frame energy of the line to 6.4 keV, a power index of the radial emissivity law β equal to −2, an inner (outer) radius of 1.26(400) R_g, and an inclination of 30°[2]. The resulting *EW* of the broad component is listed in last column of Table 1. Introducing this spectral feature significantly improved the fit statistic in 3 sources (0007+106, 0050+124, and 1116+215). As a further test we used the `GAUSS` model with σ free to vary, instead of the `LAOR` model, and iron lines with a broad profile resulted being detected in the same objects. The intensity, equivalent width, and the *F*-test for each line are shown in Table 2. In 0007+106, an iron fluorescence emission line with a broad profile was detected without the additional presence of a narrow core, while in the last two, 0050+124 and 1116+215, both the narrow and the broad emission feature are present. This limited statistic,

[1] The intrinsic width of the Gaussian line was forced to be the instrumental resolution at the given energy, $FWHM \sim 7000\ \mathrm{km\,s^{-1}}$ for both *pn* and *MOS*, $\sigma = 0$ keV.

[2] These are the same parameters used in Porquet & Reeves (2003) for the broad Fe K_α line observed in the *XMM-Newton* spectrum of the luminous quasar Q0056−363.

Table 1. Iron line properties. The table includes the name of the QSO, the best fit model of the data, the rest frame energy and intensity of the Fe K_α line modeled by a unresolved Gaussian line, the rest-frame equivalent width, the *F*-test probability, and the rest-frame equivalent width of a broad iron line modeled by a `LAOR` line.

PG Name	Model[a]	$L_{2-10\ \mathrm{keV}}$	Narrow line				Broad line
			E_{Fe}	*EW*	Intensity	*P*(*F*-test)	*EW*
		(10^{44} erg s^{-1})	(keV)	(eV)	(ph cm^{-2} s^{-1})	(%)	(eV)
0007+106⋆	A	1.4	6.4f[†]	<60	$<6\times10^{-6}$	<75	$220^{+110\,(\dagger\dagger)}_{-100}$
0050+124	E[‡]	0.78	$6.47^{+0.06}_{-0.11}$	40 ± 30	$(4\pm2)\times10^{-6}$	97.5	$100^{+40\ (\dagger\dagger)}_{-50}$
0157+001	A	0.71	6.4f	<330	$<4\times10^{-6}$	<75	<1300
0804+761	D	2.86	6.38 ± 0.06	100^{+70}_{-60}	$1.2^{+0.9}_{-0.7}\times10^{-5}$	95.7	250^{+200}_{-180}
0844+349	E	0.55	6.4f	<100	$<6\times10^{-6}$	<75	<1200
0947+396	C[‡]	2.26	$6.40^{+0.11}_{-0.07}$	120 ± 60	$3.1\pm0.2\times10^{-6}$	99.8	< 360
0953+414	E[‡]	5.41	6.4f	<50	$<4\times10^{-6}$	<75	<77
1048+342	E	1.10	$6.34^{+0.19}_{-0.04}$	100 ± 60	$1.9^{+1.1}_{-1.2}\times10^{-6}$	97.6	<160
1100+772⋆	E	11.19	$6.40^{+0.10}_{-0.04}$	60 ± 40	$3^{+3}_{-2}\times10^{-6}$	95	<110
1114+445	G	1.45	$6.45^{+0.02}_{-0.08}$	100^{+30}_{-40}	$3.3^{+1.1}_{-1.2}\times10^{-6}$	99.99	<33
1115+080	PL[‡]	65.3	6.4f	<130	$<2\times10^{-6}$	<85	1400^{+1600}_{-500}
1115+407	E	0.85	6.83 ± 0.09	130^{+80}_{-90} (<100[§])	$1.7^{+1.0}_{-0.7}\times10^{-6}$	95	<320
1116+215	C	3.1	$7.17^{+0.07}_{-0.18}$	200^{+110}_{-140} (<80[§])	$7^{+3}_{-5}\times10^{-6}$	96.5	$500^{+1100\ (\dagger\dagger)}_{-200}$
1202+281	C	2.68	6.4f	<80	$<2\times10^{-6}$	<75	<420
1206+459	PL	14.9	6.4f	<350	$<6\times10^{-6}$	<75	<580
1211+143	E	0.50	$6.45^{+0.2}_{-0.07}$	40^{+20}_{-30}	$1.7\pm1.1\times10^{-6}$	95.1	300^{+300}_{-200}
1216+069	E	4.8	6.4f	<70	$<1.6\times10^{-6}$	<75	<220
1226+023⋆	E	51.05	6.4f	<7	$<6\times10^{-6}$	<75	<17
1244+026	A	0.14	$6.65^{+0.07}_{-0.18}$	300 ± 200 (<150[§])	$7^{+5}_{-4}\times10^{-6}$	95.5	<600
1307+085	A	1.19	6.4f	<110	$<3\times10^{-6}$	<75	<920
1309+355⋆	A	0.67	$6.37^{+0.05}_{-0.06}$	180^{+80}_{-40}	$1.8^{+0.8}_{-0.4}\times10^{-6}$	99.7	<410
1322+659	C	1.08	6.48 ± 0.09	180 ± 110	$2.8^{+1.6}_{-1.7}\times10^{-6}$	97	<480
1352+183	E	1.36	$6.44^{+0.04}_{-0.07}$	150 ± 80	$4\pm2\times10^{-6}$	97.7	470^{+170}_{-300}
1402+261	C	1.4	$7.47^{+0.07}_{-0.3}$	230 ± 120 (<100[§])	$4^{+2}_{-3}\times10^{-6}$	96.4	<1200
1407+265	A	41.20	6.4f	<30	$<1.0\times10^{-6}$	<75	<66
1411+442	H	0.25	$6.43^{+0.05}_{-0.13}$	250^{+130}_{-60}	$2.9^{+1.5}_{-0.7}\times10^{-6}$	99.8	900 ± 300
1415+451	E	0.4	6.35 ± 0.07	110 ± 80	$1.5^{+1.0}_{-1.1}\times10^{-6}$	97.6	700^{+300}_{-600}
1427+480	C	1.6	$6.40^{+0.09}_{-0.2}$	90^{+50}_{-60}	$1.3^{+0.9}_{-0.8}\times10^{-6}$	97.1	<480
1440+356	D	0.58	6.4f	<80	$<3\times10^{-6}$	<60	<310
1444+407	D	1.3	6.4f	<180	$<2\times10^{-6}$	<75	1000^{+500}_{-900}
1501+106	E	0.49	6.4f	<60	$5<1\times10^{-5}$	93	<52
1512+370⋆	D	8.84	$6.52^{+0.06}_{-0.08}$	120 ± 60	$3.9^{+1.8}_{-2}\times10^{-5}$	99.5	<240
1613+658	A	1.78	6.4f	<60	$<4\times10^{-6}$	<75	<210
1626+554	D	1.46	6.4f	<160	$<7\times10^{-6}$	<75	<190
1630+377	D	20.9	$6.48^{+0.18}_{-0.11}$	600 ± 300	$5^{+3}_{-2}\times10^{-6}$	99.8	<1400
1634+706	C	127.9	6.4f	<82	$<5\times10^{-6}$	<75	<680
2214+139	I	0.48	6.34 ± 0.06	80^{+40}_{-40}	$4.0\pm1.7\times10^{-6}$	99.9	<150
2303+029	C	16.2	6.4f	<140	$<1.6\times10^{-6}$	<20	<160

(⋆) Radio loud objects. (†) In this source only an iron line with a broad profile was significantly detected. (††) The detection of the `LAOR` line at 6.4 keV is significant, i.e. *F*-test >95%. [a] Best fit model: A: blackbody; B: multicolor blackbody; C: bremsstralung emission; D: power law; E: double blackbody; F: `absori` model; G: double `absori` model + blackbody; H: partial-covering (cold) + Raymond-Smith; I: partial-covering(warm) + emission line; J: absorption + blackbody; PL: simple power law. Models with (‡) include an additional cold absorption component. All but one type of models (i.e. model PL) also include a power law component accounting for the hard X-ray band (see Piconcelli et al. 2005). The *EW* labeled with (§) correspond to the neutral iron line added in addition to the ionized one.

however, does not allow more detailed investigation of the line parameters.

For the QSOs with a significant Fe K_α emission line we also tested a model with a neutral reflection component (`PEXRAV` in XSPEC, see Magdziarz & Zdziarski 1995). This parametrization led to no significant improvement in goodness of fit in the vast majority of those sources with resulting values of $R = \Omega/2\pi$ (i.e. the solid angle subtended by the cold reflecting

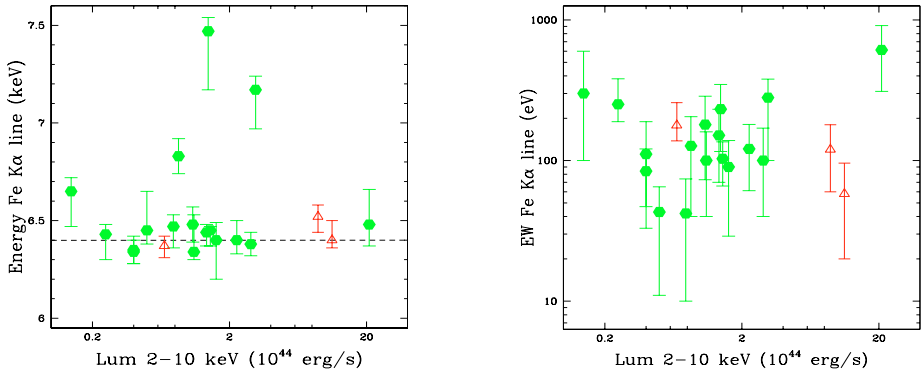

Fig. 1. a) Centroid Fe K_α line as a function of the $L_{2-10\,\mathrm{keV}}$. The radio-loud QSOs are plotted as empty triangles. **b)** Equivalent width of the narrow line significantly detected, i.e. F-test > 95%, as a function of the $L_{2-10\,\mathrm{keV}}$. The radio-loud QSOs are also plotted as empty triangles.

Table 2. Broad iron line properties. The table includes the name of the QSO for which a broad iron emission line is significant. The line was modeled by a `LAOR` line assuming a fixed rest frame energy of the line to 6.4 keV, an inner (outer) radius of 1.26(400) R_g, an inclination of 30°, and β equal to −2 (see text for further details). The intensity and rest-frame equivalent width of the broad line, as well as the F-test probability, are also given.

PG name	Intensity	EW_{broad}	$P(F\text{-test})$
	ph cm^{-2} s^{-1}	eV	%
0007+106	$(1.5 \pm 0.7) \times 10^{5}$	220^{+110}_{-100}	99.2
0050+124	$(6 \pm 3) \times 10^{-6}$	100^{+40}_{-50}	99.6
1116+215	$1.7^{+1.7}_{-1.2} \times 10^{-5}$	500^{+1100}_{-200}	97.6

material to the X-ray source located above it) basically unconstrained but consistent with zero. As expected, the bandpass (0.3–12 keV) and the limited statistics usually affecting the high energy ($E \gtrsim 8$ keV) region of the *EPIC* spectra are not suitable to constrain the strength of this bump-like emission component that peaked at ∼40 keV (Lightman & White 1988). Nonetheless, in two cases, 0007+106 and 1309+355, introduction of a reflection component significantly improved the fit at >98% confidence level with a resulting $R = 2.6^{+1.4}_{-1.2}$ and $R = 2.9^{+1.5}_{-1.1}$, respectively. Such large values of R indicates that simple slab geometry for the reprocessing medium is inadequate, compared to a partial-covering scenario with an additional spectral component emerging at high energies or an anisotropic geometry, which offer more likely explanations. The iron line parameters are not affected when the reflection model parametrization is applied.

4. Discussion

Our study reveals that about 50% of the QSOs in the sample show a significant iron fluorescent emission line in their spectra. Iron K-shell emission therefore is a common feature in the X-ray spectrum of optically-selected QSOs. In particular, we detected 20 Fe K_α lines with a narrow profile and 3 broad lines. In the following section we focus on properties of the former feature and in Sect. 4.2 discuss characteristics of the broad emission lines.

4.1. The narrow iron line

The energy centroid of all but four narrow lines (Fig. 1a) is consistent with matter in low ionization stages (FeI-XVII). The mean value of the energy for the 20 significant lines detected is 6.53 ± 0.09 keV with a dispersion lower than 0.3 keV. When only the 16 detected low ionized Fe lines are considered, the value found is $6.41^{+0.03}_{-0.04}$ keV with a dispersion lower than 0.05 keV. This best simultaneous estimate of the energy of the line and its intrinsic spread was calculated using the maximum likelihood technique of Maccacaro et al. (1988). The errors were obtained through the 68% confidence contour level. This finding turns out to contradict the *ASCA* results of Reeves & Turner (2000), who found ≳50% of the detected Fe lines at energies >6.4 keV in a sample of QSO with similar luminosities (see also George et al. 2000). Nevertheless, considering only the common objects in both samples (i.e. 0050+124, 1116+215, and 1226+023) the only minor discrepancy is found in the case of 0050+124 where an ionized line was only marginally detected in the ASCA data. The line detected in 1226+023 is not significant in none of the spectra, and the two centroid energies of 1116+215 obtained with *ASCA* and *XMM-Newton* are compatible within the errors. On the other hand, our results are compatible with other recent *XMM-Newton* studies of QSOs; in a sample of five high luminosity RQQs, Page et al. (2004c) find that the detected iron emission lines are mainly neutral. In a larger sample analysis of low–z QSOs performed with *XMM-Newton*, Porquet et al. (2004) detect an iron line in twelve out of 21 QSOs, and the values of the centroid of the Fe lines agree in all but two sources. Our finding also matches well the properties of iron K_α emission in Seyfert 1 galaxies observed with *XMM-Newton* and *Chandra*, where the mean peak of the narrow line is observed at $\langle E_{K_\alpha} \rangle \approx 6.4$ keV (Nandra et al. 1997; Yaqoob & Padmanabhan 2004).

The emission lines with energy $E_{K_\alpha} > 6.4$ keV in 1115+407 and 1116+215 are both consistent with emission due to iron at very high ionization stages (i.e. He- and H-like, respectively); while in the case of the line observed in 1402+261, the observed energy exceeds any ionization states for the K_α emission. Reeves et al. (2004) have explained the origin of this feature as a blue-shifted line originating in an accretion disk with high inclination.

The intensity of the significantly detected narrow lines appears to be independent of the X-ray luminosity for $L < 10^{45}$ erg s^{-1}, (Fig. 1b; see the next section for a more detailed discussion), with an average value $\langle EW \rangle = 80 \pm 20$ eV and an intrinsic dispersion $\sigma_{EW} < 40$ eV. Such a value is lower than 163 ± 17, i.e. the $\langle EW \rangle$ inferred by Reeves & Turner (2000) for the radio-quiet QSOs in their sample. Nevertheless, the values for the *EW* of the detected iron lines are consistent with the measurements of Page et al. (2004b) who using *XMM-Newton* data of five QSOs find *EW* values within the range 30–180 eV. The result is also compatible with the typical values found for Seyfert galaxies; the mean *EW* obtained by *ASCA* for a sample of Seyferts was 114 ± 10 eV (Nandra et al. 1997), and more recently, high resolution *Chandra* observations measured a weighted mean of 65 eV for the narrow cores (Yaqoob & Padmanabhan 2004).

The average properties of Fe K-shell narrow emission lines observed for our objects are therefore very similar to those inferred for the low-luminosity AGNs. Consequently, the origin of this feature in QSOs and Seyferts is expected to be the same. It is widely accepted that the fluorescence emission line emerges in "cold" matter distant from the central X-ray source consistent to its energy and narrow profile. Even if the emitting medium is located in the optically-thick accretion disk, regions near the radius of marginal stability for a not-rotating or spinning black hole (i.e. 6 and 1.24 gravitational radii, respectively) are ruled out. Furthermore, zones of the disk very near to the X-ray source are likely to be ionized given the high irradiation. A substantial fraction of the line flux could be due to reflection of the primary continuum off the inner walls of the torus into our line of sight (Ghisellini et al. 1994). This parsec–scale structure is a key component of AGN Unification models, and is indeed thought to subtend a large solid angle to the X-ray source (Matt et al. 2000). Assuming standard values for type 1 AGNs (i.e. a torus column density $N_{\rm H} \sim 10^{24}$ cm^{-2}, a viewing angle $\lesssim 20°$, and a half opening angle of the torus $\theta \sim 30°$), the predicted *EW* of the line produced by a torus with solar abundances is ∼100 eV (Ghisellini et al. 1994), in agreement with our observations.

Finally, we should consider the possibility of a contribution, at least partially, from the optical-to-ultraviolet Broad Line Region (BLR) to the line emission. On the basis of variability and emission properties (energy, width, *EW*), Yaqoob et al. (2001) inferred that the bulk of the iron line in NGC 5548 is indeed consistent with emission in the outer BLR. Such interpretation has been also proposed by Kaspi et al. (2002) for the Fe K$_\alpha$ line found in a very long *Chandra* HETGS observation of NGC 3783. The equivalent hydrogen column of the BLR, $N_{\rm H}$, can be estimated using the *EW* of the iron line, the index of the power law, and the fraction of sky covered by the clouds (Yaqoob et al. 2001). Considering the mean index of the power law obtained in analysis of the QSOs in the sample, $\langle \Gamma_{2-12\ \rm keV} \rangle = 1.87$ (Piconcelli et al. 2005), and the $\langle EW \rangle = 80$ eV, we get

$$N_{\rm H} \simeq 2.5 \left(\frac{0.35}{f_{\rm c}} \right) \times 10^{23}\ {\rm cm}^{-2} \quad (1)$$

where $f_{\rm c}$ is the covering factor. Assuming spherical covering, i.e. $f_{\rm c} = 1$, the equivalent hydrogen column density is $N_{\rm H} \simeq 9 \times 10^{22}$ cm^{-2}. This value can be considered as a lower limit to the absorption column and is, therefore, in agreement with typical values of BLR clouds, i.e. $N_{\rm H} \simeq 10^{23}$ cm^{-2}.

Emission lines from ionized iron (i.e. with an energy >6.4 keV) can be produced by reflection in an ionized accretion disk (e.g. Reeves et al. 2001) or, alternatively, by warm scattering material along the line of sight (Bianchi et al. 2004). The latter mechanism also appears likely in the case of 1116+215, for which the presence of a warm medium is suggested by the detection of warm absorber signatures in the soft X-ray portion of the spectrum (Piconcelli et al. 2005). Similarly, the strength of the Fe line in 2214+139 is consistent with an origin in the low-ionization component of the two-zone warm absorber observed in this source (Piconcelli et al. 2004).

4.2. The broad iron line

In contrast to the narrow Fe K$_\alpha$ emission line detected in 20 of the sources, the broad component seems to be less common in QSOs with only 3 out of 38 significant detections.

Emission from an accretion disk reaching down to a few gravitational radii of the black hole is the most likely explanation for iron K$_\alpha$ lines with a broad profile. Such a skewed velocity profile indeed suggests that fluorescence takes place in a strong gravity regime (see Fabian et al. 2000, for a review). Except for a very few remarkable cases (Porquet & Reeves 2003; Comastri et al. 2004), most of the detected relativistic iron lines have been detected in nearby Seyfert-like AGNs (Nandra et al. 1997). Their presence in QSOs appears to be rare, which has been interpreted as evidence of different physical properties of the accretion disk in these objects, such as high ionization or small transition radius to radiatively inefficient accretion flows. Nevertheless a selection effect due to the poor statistical quality of most X-ray quasar spectra must be borne in mind, and detection of broad Fe lines in three quasars of our sample therefore appears noteworthy.

The broad features observed in 0007+106 and 0050+124 could also be explained as contributions from different iron lines at different ionization levels as suggested by the presence of some positive data-to-ratio residuals in the range 6–7 keV (see also Gallo et al. 2004). However, current *XMM-Newton* data does not allow us to investigate this hypothesis further. Similarly, the limited signal-to-noise of the observation of 1116+215 hampers a detailed analysis of the broad iron lines and affects the significance of the inferred spectral parameters, i.e. leaving almost unconstrained the value of the line intensity ($EW = 500^{+1100}_{-200}$ eV).

4.2.1. Behavior of the *EW* with $L_{2-10\ \rm keV}$

The Baldwin effect was first reported in the optical and ultraviolet emission lines of QSOs. Baldwin (1977) observed a decrease in the equivalent width of the C$_{\rm IV}$ emission line with increasing ultraviolet luminosity. This anticorrelation between the luminosity and the equivalent width was also found in the

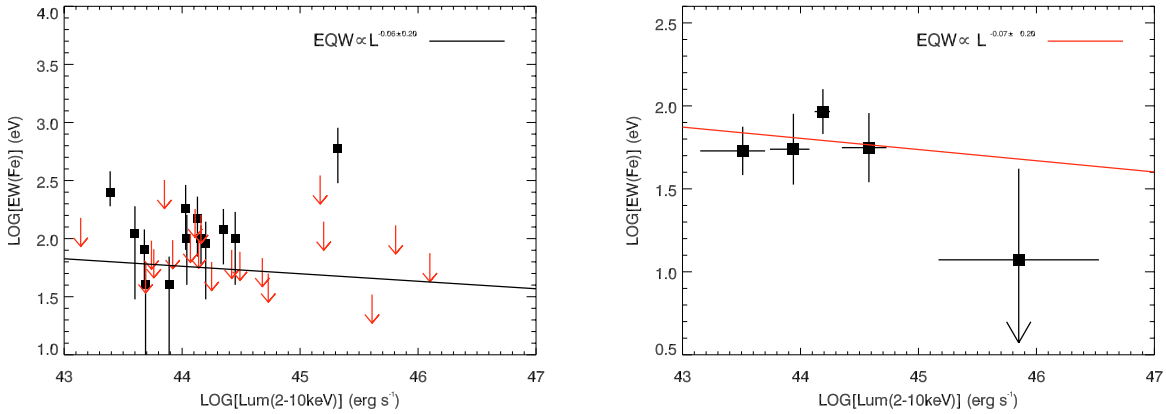

Fig. 2. Relation between the equivalent width of the Fe K$_\alpha$ line and the $L_{2-10\ \mathrm{keV}}$ for the radio quiet quasars. (*Upper panel*) The plot includes measurements for each set of data. The solid line shows the fit to all the detections while for the dashed line only the significant detections are considered. (*Lower panel*) The plot represents all measurements binned in five groups. The solid lines show the fit to the five points.

X-ray band for the Fe K$_\alpha$ emission line. Iwasawa & Taniguchi (1993) studied 37 AGNs observed with *Ginga* and found the relation $EW(\mathrm{Fe\ K}_\alpha) \propto L_{2-10\ \mathrm{keV}}^{-0.20\pm0.03}$. A similar study of 39 AGNs performed with *ASCA* also confirmed this effect (Nandra et al. 1997). More recently, Page et al. (2004a) obtained a relation of $EW(\mathrm{Fe\ K}_\alpha) \propto L_{2-10\ \mathrm{keV}}^{-0.17\pm0.08}$ for a sample of 53 type I AGNs observed with *XMM-Newton*.

In Fig. 2, we show the relation between the 2–10 keV luminosity and the equivalent width of the narrow Fe K$_\alpha$ line for the objects in our sample. In order to avoid mixture with RLQs, where hard X-ray emission could be *contaminated* by the relativistic jet components, we have considered here only RQQs.

Several different techniques have been compared to study the behavior of the *EW* with luminosity.

First, linear regressions of $\log EW$ versus $\log L_{2-10\ \mathrm{keV}}$ were performed using ASURV (*Astronomy Survival Analysis*, Feigelson & Nelson 1985) package. ASURV facilitates a correct statistical analysis when censored data (upper limits in this case) are present, although errors are not considered in the calculations (see below). This allows us to study the relationship between *EW* and $L_{2-10\ \mathrm{keV}}$, including all significant and non-significant (the upper limits) detection of the neutral narrow lines. For the four ionized lines found in the analysis, an extra neutral component was added to the fit model. This component, modeled by a Gaussian line with $\sigma = 0$, is not significantly required in any of the four sources. The upper limits of the corresponding *EW*s can also be found in Table 1.

Within the ASURV package, we performed a Spearman-Rank test considering the detections and upper limits, and found only a 30% probability that $\log EW$ and $\log L_{2-10\ \mathrm{keV}}$ are correlated. The fit calculated with the Buckley-James method gives a power law index of $\alpha = -0.06 \pm 0.20$, where $EW(\mathrm{FeK}_\alpha) \propto L_{2-10\ \mathrm{keV}}^{\alpha}$. The result obtained by Page et al. (2004a) with the same method, $\alpha = -0.17 \pm 0.08$, is compatible with our value within the errors.

The disadvantage of using the ASURV package in the data analysis is that actual detections are considered without taking errors into account, thereby underestimating the uncertainties in determining the slope in certain cases. In order to avoid this problem, we calculated the mean *EW* in five different luminosity bins with a similar number of objects in each bin, therefore we studied the relationship between *EW* and $L_{2-10\ \mathrm{keV}}$ using these five bins. The weighted mean *EW*s were calculated considering asymmetric errors statistics (Barlow 2004). The index of the power law obtained is $\alpha = -0.07 \pm 0.20$, very similar to the results given by ASURV when upper limits are considered in the fit. Figure 2b shows the data together with the fit.

Figure 3 shows a comparison of the data-to-continuum residuals in the 4.5–7 KeV energy band, obtained by combining the ratios corresponding to objects selected in five luminosity intervals. For each interval, we considered the best fit model of each QSO but excluded the iron line in cases where it is significantly detected. The unbinned data-to-model ratio of each QSO is translated into the rest frame and grouped in bins of 0.2 keV size. Each plot also includes a Gaussian emission line broadened to the intrinsic resolution of the *pn* at the energy of the iron line, i.e. *FWHM* = 150 eV. The plots show residuals compatible with the neutral iron line being narrow. The residuals in the last bin are larger and randomly distributed.

An anticorrelation between *EW* and hard X-ray luminosity is also compatible with our data. However, other behaviors different from a power law cannot be ruled out. The data actually suggest a constant *EW* for $L_{2-10\ \mathrm{keV}} \lesssim 10^{45}$ erg s^{-1} and a stepwise decrease above this threshold. As can be seen in Fig. 2b the anticorrelation between *EW* and $L_{2-10\ \mathrm{keV}}$ is actually determined mainly by the highest luminosity bin.

The physical origin of variation in the iron line equivalent width with luminosity is related to where the line is originated. Assuming that the Fe K$_\alpha$ line is produced by fluorescence, various scenarios have been proposed. Iwasawa & Taniguchi (1993) suggested that the emission line is produced in the clouds of the Broad Line Region. The X-ray primary emission ionizes these clouds explaining the observed decrease in the equivalent width with luminosity. Nandra et al. (1997) proposed that for iron lines, which are most likely produced in the accretion disk, an increasing degree of ionization with luminosity could also account for the Baldwin effect. Assuming the emission line is originated in the torus, Page et al. (2004a) suggested that increasing X-ray emission could cause a decrease

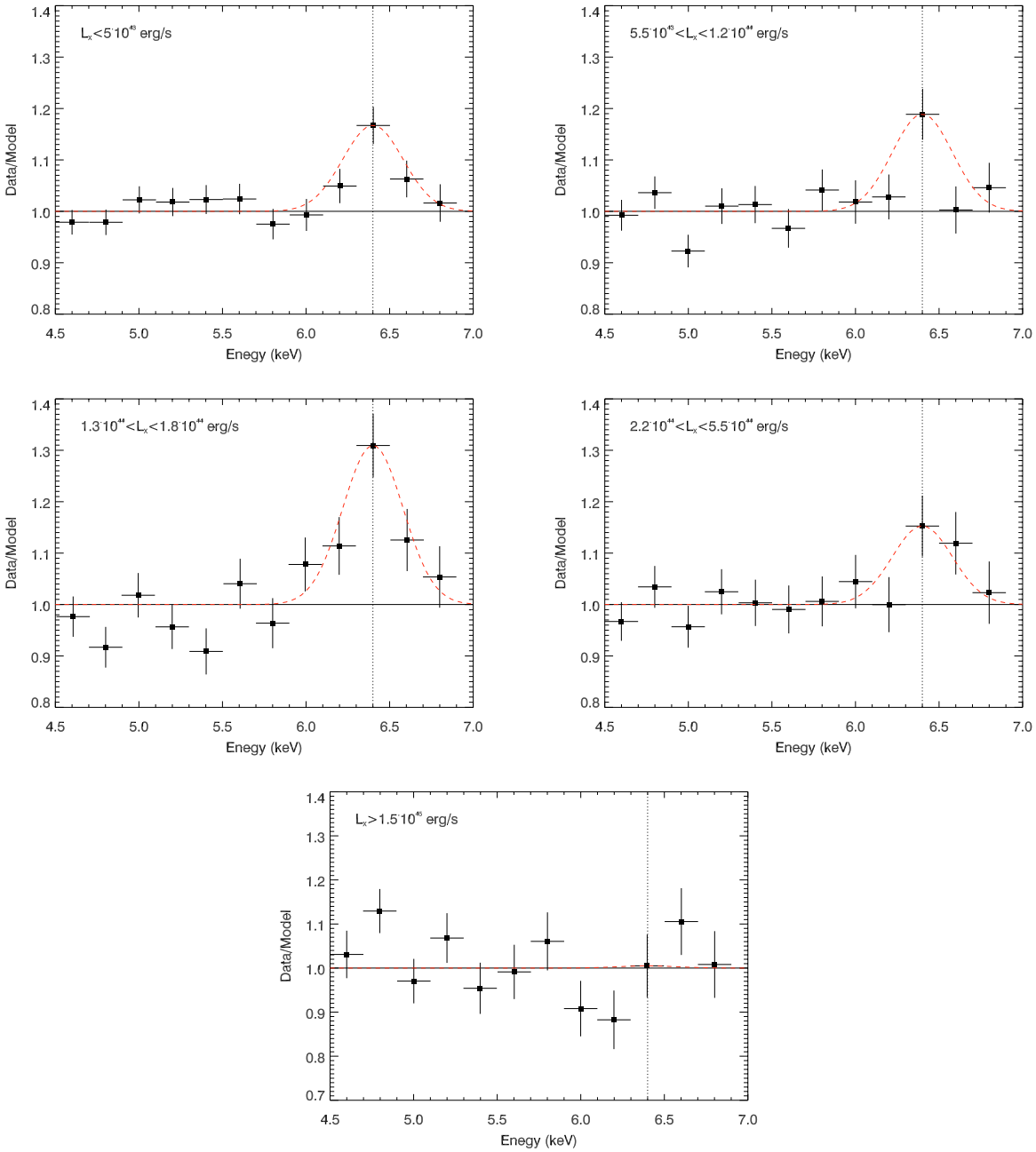

Fig. 3. Mean data-to-model ratios in five luminosity bins, assuming for each QSO the best fit model and excluding the iron line and correcting by redshift. The observed lines represent a Gaussian profiles with centroid energy 6.4 keV, and width equal to the intrinsic *pn* resolution, normalized to the 6.4 keV data point.

in the covering factor of the torus and hence a decrease in the equivalent width of the iron line. A step function behavior of the value of *EW* with luminosity favors our explanation in terms of the increase in the degree of ionization suggested by Iwasawa & Taniguchi (1993). When the material reaches a particular ionization state, the emission line could be suppressed by resonant trapping and/or full electron stripping and the *EW* would then abruptly decrease. In such a case, the material where the line is emitted should be most likely identify with the BLR or accretion disk. In the last case, the average unresolved profile indicates an origin in the outermost regions of the accretion disk.

Nevertheless, our analysis cannot rule out a smooth power law dependence, $EW(\mathrm{FeK}_\alpha) \propto L^{\alpha}_{2-10\ \mathrm{keV}}$, as suggested by Page et al. (2004a). The slope of the power law ranges between −0.27 and 0.14, taking into account the different analysis and their corresponding uncertainties. More highly luminous QSO with high signal-to-noise need to be added to this analysis to reduce large uncertainties in determining the slope. A possible divergence from previous works could be due to a selection effect, as they claim the presence of X-ray Baldwin effect and include both RQQs and RLQs in their sample. In particular, most of the objects with high luminosity, $L_{2-10\ \mathrm{keV}} > 10^{45}$ erg s^{-1}, were radio loud. However, as shown

by Reeves & Turner (2000), there is a strong anticorrelation between iron K_α *EW* and radio loudness. This hypothesis is also strongly supported by anticorrelation between radio loudness and the strength of the soft excess component studied in Piconcelli et al. (2005). This trend could be due to the likely presence of an additional jet emission component that weakens the strength of the iron line. Inclusion of RLQs in the highest 2–10 keV luminosity bins in previous works could therefore have affected the results on the X-ray Baldwin effect. The choice of our sample minimizes this bias.

A similar analysis of the radio loud objects is hampered due to the low number of RLQs in the sample. Furthermore, a significant Fe K_α line was detected in only one out of five RLQs.

5. Summary and conclusions

We present here an analysis of the K_α fluorescent iron emission line in the *XMM-Newton* spectra of 38 PG QSOs, including the presence and properties of emission lines with both narrow and broad profiles.

A narrow unresolved (i.e. $FWHM \leq 7000\,\mathrm{km\,s^{-1}}$) emission Fe K_α line was detected in ∼50% of the objects studied. The energy centroids indicate that the majority of the lines originated in cold material (Fe I–XVII). The mean equivalent width for the narrow line is $\langle EW \rangle = 80^{+30}_{-20}$ eV with a dispersion $\sigma_{EW} < 40$ eV. Such properties are consistent with several scenarios for the origin of the line. Fluorescence likely occurs in the outermost parts of the accretion disk and/or in even more external regions, such as the molecular torus or the clouds of the Broad Line Region. For two objects, i.e. 1115+407 and 1116+215, the line energies are associated with the highest ionization stages of iron, suggesting emission from an ionized accretion disk, due to scattering by warm material located in the line of sight or due to the presence of an outflow.

We also investigated the presence of an X-ray Baldwin effect for the Fe K_α line of the RQQs. The RLQs were excluded in order to avoid possible contamination from a relativistic jet component in the X-ray emission, which could have biased the anticorrelations published in the literature prior to our study. However, no clear correlation was found between strength of the iron line and 2–10 keV luminosity. Assuming a power law behavior $EW(\mathrm{FeK}_\alpha) \propto L^{\alpha}_{2-10\ \mathrm{keV}}$, α turned out to in the range between −0.3 and 0.14.

Broad relativistic lines were detected in three objects, less than 10% of the QSOs in the sample. These objects have low luminosities ($L_{2-10\ \mathrm{keV}} \lesssim 10^{44}$ erg s^{-1}) suggesting a possible anticorrelation between the X-ray luminosity (hence the ionization state of the uppermost disk layers) and the strength of lines originating in the disk, as has been proposed by Nayakshin et al. (2000). However, a selection effect due to limited statistics affecting the most distant (very luminous) QSOs prevents us from drawing firm conclusions on this point.

After comparing our results with those of recent *XMM-Newton* and *Chandra* observations of Seyfert galaxies, it seems that characteristics of the Fe K-shell emission lines detected in the spectra do not significantly change as a function of the X-ray luminosity. We report average values of the *EW* and the energy centroid of the line which are both consistent with those in Seyfert galaxies. Moreover, Piconcelli et al. (2005) also found a similarity between the properties of the cold and warm absorption in QSOs and Seyfert galaxies. Our analysis therefore allows an extension of the well studied observational properties of the nearby X-ray bright Seyferts to the QSO realm, at least for those optically selected.

Acknowledgements. The authors would like to thank the referee, Dr. James Reeves, for this encouraging report and useful comments, which improved the paper significantly. We also thank the *XMM-Newton* SOC science support team members. This paper is based on observations obtained with *XMM-Newton*, an ESA science mission with instruments and contributions directly funded by ESA Member States and the USA (NASA). This research has made use of the NASA/IPAC Extragalactic Database (NED) operated by the Jet Propulsion Laboratory, California Institute of Technology, under contract with the National Aeronautics and Space Administration.

References

Arnaud, K. A. 1996, Astronomical Data Analyis and Systems, ASP Conf. Ser., 101, 17
Baldwin, J. A. 1977, ApJ, 214, 679
Barlow, R. 2004 [physics/0406120]
Bennett, C. L., Hill, R. S., Hinshaw, G., et al. 2003, ApJS, 148, 97
Bianchi, S., Matt, G., Balestra, I., Guainazzi, M., & Perola, G. C. 2004, A&A, in press
Chartas, G., Brandt, W. N., & Gallagher, S. C. 2003, ApJ, 595, 85
Comastri, A., Brusa, M., & Civano, F. 2004, MNRAS, 351, L9
Fabian, A. C. 2002, X-ray astronomy in the new millennium, ed. R. D. Blandford, A. C. Fabian, & K. Pounds, Roy. Soc. London Phil. Tr. A, 360, 2035
Fabian, A. C., Iwasawa, K., Reynolds, C. S., & Young, A. J. 2000, PASP, 112, 1145
Feigelson, E. D., & Nelson, P. I. 1985, ApJ, 293, 192
Gallo, L. C., Boller, T., Brandt, W. N., Fabian, A. C., & Vaughan, S. 2004, A&A, 417, 29
George, I. M., Turner, T. J., Yaqoob, T., et al. 2000, ApJ, 531, 52
George, I. M., & Fabian, A. C. 1991, MNRAS, 249, 352
Ghisellini, G., Haardt, F., & Matt, G. 1994, MNRAS, 267, 743
Ghisellini, G., Maraschi, L., & Treves, A. 1985, A&A, 146, 204
Haardt, F., & Maraschi, L. 1993, ApJ, 413, 507
Iwasawa, K., & Taniguchi, Y. 1993, ApJ, 413, L15
Kaspi, S., Brandt, W. N., George, I. M., et al. 2002, ApJ, 574, 643
Krolik, J. H., Madau, P., & Zycki, P. T. 1994, ApJ, 420, L57
Laor, A., Fiore, F., Elvis, M., Wilkes, B. J., & McDowell, J. C. 1997, ApJ, 477, 93
Lightman, A. P., & White, T. R. 1988, ApJ, 335, 57
Maccacaro, T., Gioia, I. M., Wolter, A., Zamorani, G., & Stocke, J. T. 1988, ApJ, 326, 680
Magdziarz, P., & Zdziarski, A. A. 1995, MNRAS, 273, 837
Makishima, K. 1986, Lect. Notes Phys., 266, 246
Matt, G., Perola, G. C., & Piro, L. 1991, A&A, 247, 25
Matt, G., Fabian, A. C., Guainazzi, M., et al. 2000, MNRAS, 318, 173
Mushotzky, R. F., Serlemitsos, P. J., Boldt, E. A., Holt, S. S., & Becker, R. H. 1978, ApJ, 220, 790
Nandra, K., George, I. M., Mushotzky, R. F., Turner, T. J., & Yaqoob, T. 1997, ApJ, 488, L91

Nandra, K., & Pounds, K. A. 1994, MNRAS, 268, 405
Nayakshin, S., Kazanas, D., & Kallman, T. R. 2000, ApJ, 537, 833
Page, K. L., O'Brien, P. T., Reeves, J. N., & Turner, M. J. L. 2004a, MNRAS, 347, 316
Page, K. L., Schartel, N., Turner, M. J. L., & O'Brien, P. T. 2004b, MNRAS, 352, 523
Page, K. L., Reeves, J. N., O'Brien, P. T., Turner, M. J. L., & Worrall, D. M. 2004c, MNRAS, 353, 133
Piconcelli, E., Jimenez-Bailón, E., Guainazzi, M., et al. 2004, MNRAS, 351, 161
Piconcelli, E., Jiménez-Baión, E., Guainazzi M., et al. 2005, A&A, 432, 15
Porquet, D., Reeves, J. N., O'Brien, P., & Brinkmann, W. 2004, A&A, 422, 85
Porquet, D., & Reeves, J. N. 2003, A&A, 408, 119
Pounds, K. A., & Reeves, J. N. 2002 [arXiv:astro-ph/0201436]
Reeves, J. N., & Turner, M. J. L. 2000, MNRAS, 316, 234
Reeves, J. N., Turner, M. J. L., Ohashi, T., & Kii, T. 1997, MNRAS, 292, 468
Reeves, J. N., Turner, M. J. L., Pounds, K. A., et al. 2001, A&A, 365, L134
Reeves, J. N., Porquet, D., & Turner, M. J. L. 2004 [arXiv:astro-ph/0408403]
Reynolds, C. S., & Nowak, M. A. 2003, Phys. Rep., 377, 389
Ross, R. R., Fabian, A. C., & Young, A. J. 1999, MNRAS, 306, 461
Sambruna, R. M., Eracleous, M., & Mushotzky, R. F. 1999, ApJ, 526, 60
Schmidt, M., & Green, R. F. 1983, ApJ, 269, 352
Tanaka, Y., Nandra, K., Fabian, A. C., et al. 1995, Nature, 375, 659
Wilms, J., Reynolds, C. S., Begelman, M. C., et al. 2001, MNRAS, 328, L27
Yaqoob, T., & Padmanabhan, U. 2004, ApJ, 604, 63
Yaqoob, T., George, I. M., Nandra, K., et al. 2001, ApJ, 546, 759
Yaqoob, T., George, I. M., Nandra, K., et al. 1999, ApJ, 525, L9